Effects of S-doping on the electronic transition, band gap, and optical absorption of GaSe$_{1-x}$S$_x$ single crystals

Tingting Sha [a], Wenwu Li [a, *], Shiyou Chen [a], Kai Jiang [a], Jiajun Zhu [a], Zhigao Hu [a], Zhiming Huang [b], Junhao Chu [a], Konstantin A. Kokh [c], Yury M. Andreev [d, e]

[a] Key Laboratory of Polar Materials and Devices (Ministry of Education), Technical Center for Multifunctional Magneto-Optical Spectroscopy (Shanghai), East China Normal University, 500 Dongchuan Road, Shanghai, 200241, China
[b] National Laboratory for Infrared Physics, Shanghai Institute of Technical Physics, Chinese Academy of Science, 420 North Zhongshan Road, Shanghai, 200083, China
[c] Laboratory of Crystal Growth, Institute of Geology and Mineralogy SB RAS, 3, Koptyuga Ave., 630090, Novosibirsk, Russia
[d] Laboratory of Infrared Lasers, High Current Electronics Institute SB RAS, 2/3, Akademicheskii Ave., Tomsk, 634055, Russia
[e] Laboratory of Geosphere-Biosphere Interactions, Institute of Monitoring of Climatic and Ecological Systems SB RAS, 10/3 Akademicheskii Ave., Tomsk, 634055, Russia

ARTICLE INFO

ABSTRACT

The intrinsic evolutions of electronic transition and the band gap of GaSe$_{1-x}$S$_x$ solid solution single crystals ($x = 0$, 0.133, and 0.439) grown for nonlinear optical applications have been systemically investigated by using spectroscopic ellipsometry and first-principle calculations. Five interband electronic transitions E_1, E_2, E_3, E_4, and E_5 have been obtained by fitting the second derivatives of the complex dielectric functions and the physical origins were explained with the aid of theoretical calculations. It is found that the interband electronic transition energy E_2, E_3, and E_4 show a blueshift trend from 3.457 eV, 3.736 eV, and 4.810 eV at $x = 0$ to 3.786 eV, 4.628 eV, and 5.086 eV at $x = 0.439$, respectively. This is because the larger Se atoms are replaced by smaller S atoms in GaSe$_{1-x}$S$_x$. The experimental band gap of GaSe$_{1-x}$S$_x$ is increased from 1.908 eV at $x = 0$ to 2.081 eV at $x = 0.439$. Moreover, in order to verify the influences of S-doping on the band gap of GaSe$_{1-x}$S$_x$, we performed the first-principle calculations based on the density-functional theory. The theoretical results also confirm that the band gap energy increases from 2.085 eV at $x = 0$ to 2.15 eV at $x = 0.439$, which is in good agreement with the experiment results.

© 2017 Elsevier B.V. All rights reserved.

1. Introduction

Two-dimensional (2D) van der Waals semiconductors such as graphene and transition metal dichalcogenides have attracted significant attention from the scientific community in the past ten years. Their unique mechanical, electronic, and optical properties hold great potential for harnessing them as key components in novel applications for valleytronic, electronics and optoelectronics. [1–4]. For example, 2D materials have atomic thickness, sizable bandgap, mechanical flexibility, high charge mobility, and high chemical stability [5,6]. As a typical 2D material, GaSe has attracted considerable attention because of its optical and structural properties that have been found very attractive for laser frequency

conversion by means of nonlinear optics. Besides, GaSe is found to be a good matrix material for doping with various elements to modify optical and mechanical properties. The observation of the exciton and biexciton transition renders quantum emitters in nanoscale GaSe potential candidates for entangled photon resonances [7,8].

Recently, many efforts have been made to study the band gap, electronic transition, optical absorption, and mechanical properties of the GaSe doped by other elements, such as Al, In, Te [8–10]. Previous reports demonstrated weakly modified properties due to large differences in atomic sizes, leading to a rapidly lattice degradation at doping level of a few at%. Among different doping elements, S doped GaSe is interesting because S and Se atoms are isovalent, possess similar size and can form isostructural binary compounds. As a result, solid solution crystal GaSe:GaS or GaSe$_{1-x}$S$_x$ can be grown with large mixing ratio x and hence strongly modified physical properties. GaSe$_{1-x}$S$_x$ had been

proposed to possess the potential abilities for the optoelectronic, mid-IR and terahertz devices in a wide photon energy range. In our previous works, GaSe$_{1-x}$S$_x$ single crystals with $x \leq 0.44$ (11 at% S) doping have been widely used as nonlinear materials for mid-IR and THz generation. Up to 15 times higher efficiency in mid-IR generation than that for pure GaSe was demonstrated due to improved optical quality and increased damage threshold, as well as higher efficiency in THz generation [9]. Therefore, it is reasonable to further investigate the physical properties of solid solution GaSe$_{1-x}$S$_x$ in order to fully exploit its wider potential applications as a nonlinear material.

GaSe$_{1-x}$S$_x$ has been proposed to possess the potential abilities for the optoelectronic and terahertz devices in a wide photon energy range. Therefore, optical properties such as dielectric function, absorption coefficient, optical band gap, and electronic band structure of GaSe$_{1-x}$S$_x$ are key parameters for device applications. Many structural characterization methods such as XRD, AFM, SEM, EDS, and TEM have been used to investigate the crystalline structure, surface morphology, and cross-sectional microstructures of solid state materials. [11—17]. Furthermore, many optical techniques, such as Raman scattering, photoluminescence, and infrared spectroscopy, have been used to study the lattice vibrations, electronic transitions, and band gap of 2D materials. Among them, spectroscopic ellipsometry (SE) is a nondestructive and powerful technique to investigate the optical band gap, dielectric constants, and electronic transitions of materials. On the other hand, the first-principle calculation of electronic and optical properties based on density functional theory (DFT) can be used to explain the experimental results and physical origins of the optical features [8]. First-principle calculation results reveal that the band gap of GaSe$_{1-x}$S$_x$ could be influenced upon doping with S [18].

In this work, the optical properties and electronic band structure of GaSe$_{1-x}$S$_x$ ($x = 0$, 0133, and 0.439) single crystals have been studied by comparison of using spectroscopic ellipsometry and first-principle calculations. The optical constants, optical band gap, and electronic transitions with different S concentrations have been explored. Moreover, the origins of the interband transitions have been uniquely assigned and the evolution of band gap with different concentrations of S-doping has been discussed.

2. Experimental details

GaSe$_{1-x}$S$_x$ ($x = 0$, 0.133, and 0.439) single crystals were grown by modified syntheses and growth techniques. The starting materials for the synthesis were Ga 99.9997, Se 99.99, and S 99.95, which were additionally purified by remelting in the continuously evacuated ampoule. In this work, synthesis ampoules were loaded up to unusual 65% in the volume to minimize the quantity of and interaction with rest gases. The Ga, Se, and S (nominal 3 at% or 11 at%) were weighed in stoichiometric ratio with a accuracy of about ±0.1 mg. The mixing ratio x should be calculated as:

$$x = \frac{0.01\text{at}\%_{Te,S}(A_{Ga} + A_{Se})}{A_{Te,S} + 0.01\text{at}\%_{Te,S}(A_{Se} - A_{Te,s})}, \tag{1}$$

where A is atomic weight. According to Equation (1), 3 at% S-doped GaSe is identical to solid solution GaSe$_{1-x}$S$_x$ with $x = 0.133$, while 11 at% S-doped GaSe is identical to solid solution GaSe$_{1-x}$S$_x$ with $x = 0.439$. We synthesized the charges in the single-zone furnace.

For the growth process, the polycrystalline material was loaded into a single wall quartz ampoule. Crystal growth was performed by the vertical Bridgman method with heat field rotation. The growth ampoule was sealed at 10^{-4} Tor and put into the furnace having a temperature gradient of ~15 K above estimated level of crystallization front. After homogenization of the melt at the temperature

of 30 K above the melting point, the ampoule was mechanically lowered at the speed of 10 mm/day. The internal surface of the ampoule had a layer of pyrolytic carbon which protected the melt from contact with the walls. The details of the growth process can be found else-where [19].

Thick samples, about 3 mm, GaSe$_{1-x}$S$_x$ ($x = 0$, 0.133, and 0,439) were made for experimental study by cleaving from single crystalline boules of 28 mm in diameter and 80 mm long boules and used without any additional processing. The crystals were cleaved readily along the (0001) plane. With careful preparation, automatically flat surfaces along this direction were produced. The X-ray diffraction patterns were obtained with a XRD-6000 diffractometer (Shimadzu, Japan) operating with the Cu Kα radiation. The diffraction data were collected from about 10 to 50° of the 2θ angular range with a step of 0.03° and accumulation time of 1 s per step. Scanning electron microscopy (SEM Quanta 200 3D microscope, FEI, Netherlands) in combination with energy-dispersive X-ray spectroscopy (EDS, EDAX ECON VI microanalyzer) were used to measure Ga, Se and S contents as well as unpredictable impurities. Surface roughness was measured by a Probes HOMMEL-ETAMIC T1000 (JENOPTIK AG, Germany) profilometer. Transmission electron microscope (TEM) CM12 (Philips, Netherlands) were employed to analyze the structure.

The spectroscopic ellipsometry experiments were carried out by the vertical variable-angle near infrared-ultraviolet ellipsometer (V-VASE, USA,J.A. Woollam Co., Inc.) in the incident angle 70° and in the photon energy range of 1.03—6.52 eV (190—1200 nm) with a spectral resolution of 5 nm. Band structure and dielectric constant were calculated with DFT as implemented in the Vienna Ab Initio Simulation Package code [20]. Local density approximation (LDA) exchange correlation potential was used in all the calculations [21]. The projector augmented-wave pseudopotentials [22] were used with 450 eV energy cutoff of plane-wave basis. LDA usually underestimates the band gap. So, we used the modified Becke-Johnson exchange [23,24] in combination with LDA to describe the band gaps of these compounds, which can generate band gaps with an accuracy similar to hybrid functional or Green's function and Coulomb interaction method and can be computationally less expensive.

3. Results and discussion

3.1. Structure analysis

GaSe and GaS single crystals belong to III—VI semiconductors. Its multilayer bulk structure is formed by four-atomic-sheet Se-Ga-Ga-Se primitive layers. The strong bonds inside the layers are thought to be mainly covalent with some ionic contribution, however, the inter-layer bonding is much weaker and mainly of van der Waals force. When S is doped into GaSe, the structure of GaSe$_{1-x}$S$_x$ is formed by partial replacement of Se for S atoms. The side view and top view of the GaSe layer structure can be seen from Fig. 1(a) and (b), respectively. The primitive unit cell extends over two layers of GaSe and contains four Ga and four Se atoms. In each layer two monoatomic sheets of Ga are sandwiched between two monoatomic sheets of Se.

The XRD results of GaSe$_{1-x}$S$_x$ ($x = 0$, 0.133, and 0.439) single crystals are shown in Fig. 2. Four diffraction peaks (002), (004), (006), and (008) can be observed from the pattern, which indicates that all three samples exhibit single crystal structures. Compared with the results of undoped GaSe single crystal, a weaker peak (006) arises from S doped GaSe samples. Furthermore, all of the diffraction peaks shift toward the larger diffraction angle with increasing the S concentration. This result confirms that the S has been successfully incorporated into the GaSe matrix lattice.
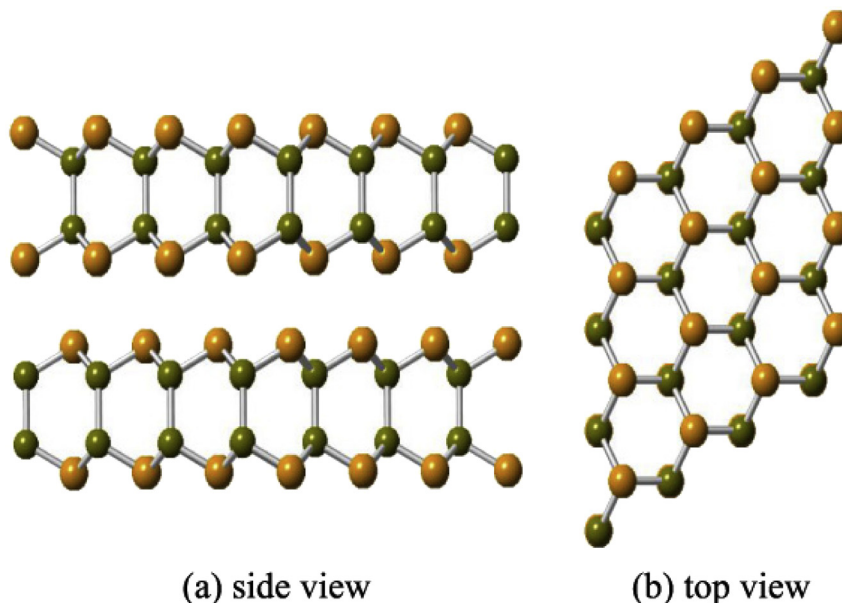
Fig. 1. Schematic view of the crystal structure of GaSe from (a) side view and (b) top view.
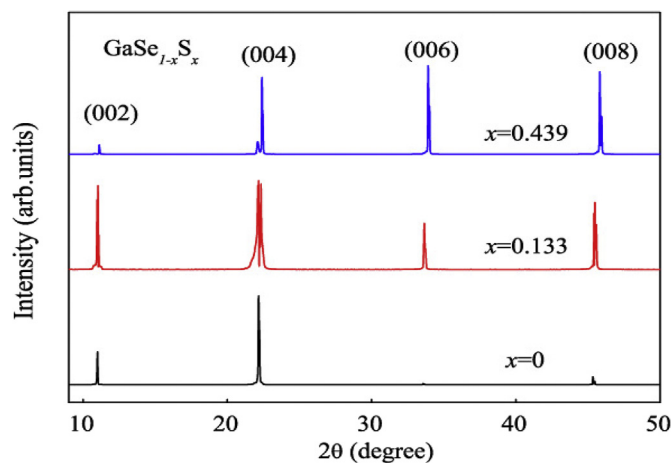

Fig. 2. The XRD pattern of GaSe$_{1-x}$S$_x$ (x = 0, 0.133, and 0.439) single crystals.

Figs. 3 and 4 show the SEM and TEM images of the GaSe$_{1-x}$S$_x$ single crystals with different S concentrations, respectively. From Fig. 3, the 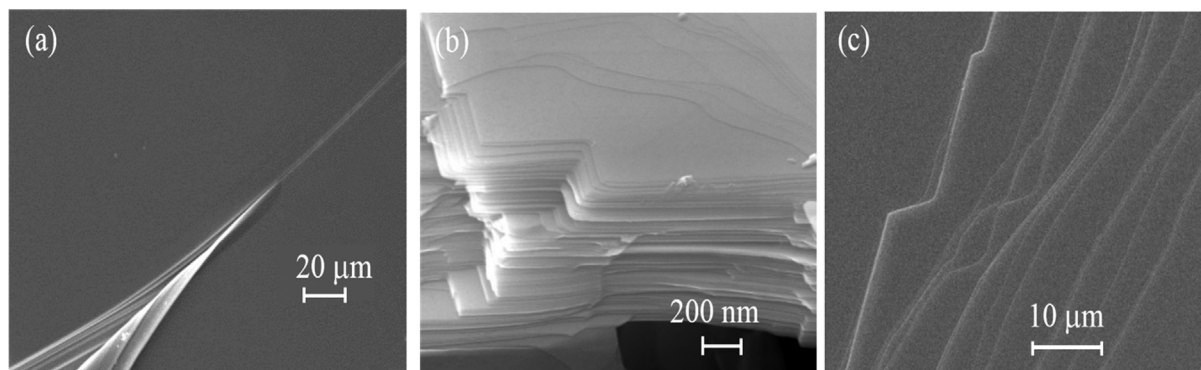layered structure of all samples can be seen clearly. All of the samples have high quality structural property and optical quality surfaces with small grain sizes, which indicate that the layered structures of the manufactured GaSe$_{1-x}$S$_x$ samples are similar to that for GaSe sample. The estimated surface roughness is as low as ≤0.15 nm. This is somewhat smaller than that for the doped crystals, which correlates well with improvement in optical quality with the S-doping. The surfaces of the samples are smooth and free of precipitates, voids, and micro bubbles. High-quality and identical structural properties can be also confirmed from TEM patterns (see Fig. 4).

The EDS spectra of the single crystals are shown in Fig. 5. The body of the GaSe$_{1-x}$S$_x$ single crystals is composed of Ga, Se, and/or S elements. It can be found that the intensities of S peak increase with increasing the S content. This confirms again that the S has been successfully incorporated into the GaSe crystals. The chemical composition of the grown GaSe$_{1-x}$S$_x$ crystals well coincides with the growth charge composition, and the crystals do not contain unpredicted impurities. Therefore, high structural-quality and optical-quality crystals with the expected chemical compositions were grown, and the samples with high optical-quality surfaces were manufactured for ellipsometric study.

Fig. 3. SEM images of GaSe$_{1-x}$S$_x$ single crystals: (a) top view on GaSe sample with laser-blade-cut surface, (b) side view on GaSe$_{0.867}$S$_{0.133}$ sample, and (c) top view on GaSe$_{0.561}$S$_{0.439}$ sample with broken layers on the surface.
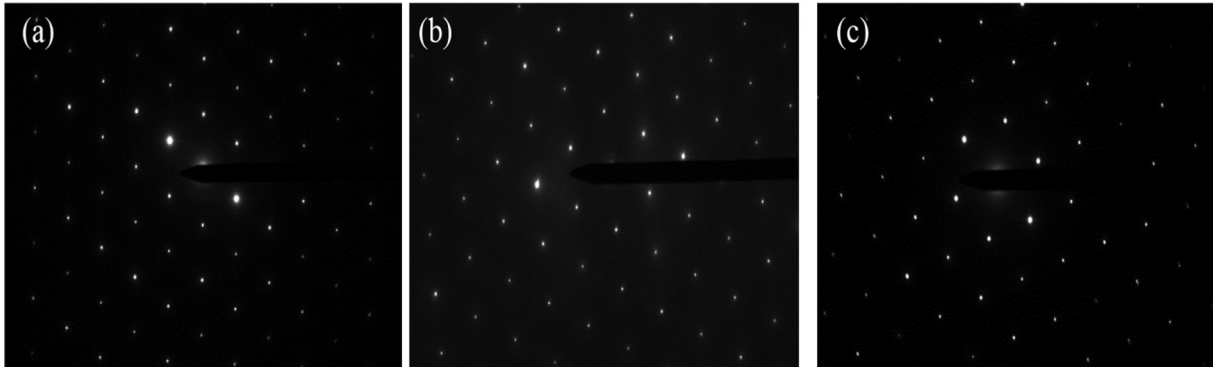
Fig. 4. TEM patterns for (a) GaSe, (b) GaSe$_{0.867}$S$_{0.133}$, and (c) GaSe$_{0.561}$S$_{0.439}$ single crystals.
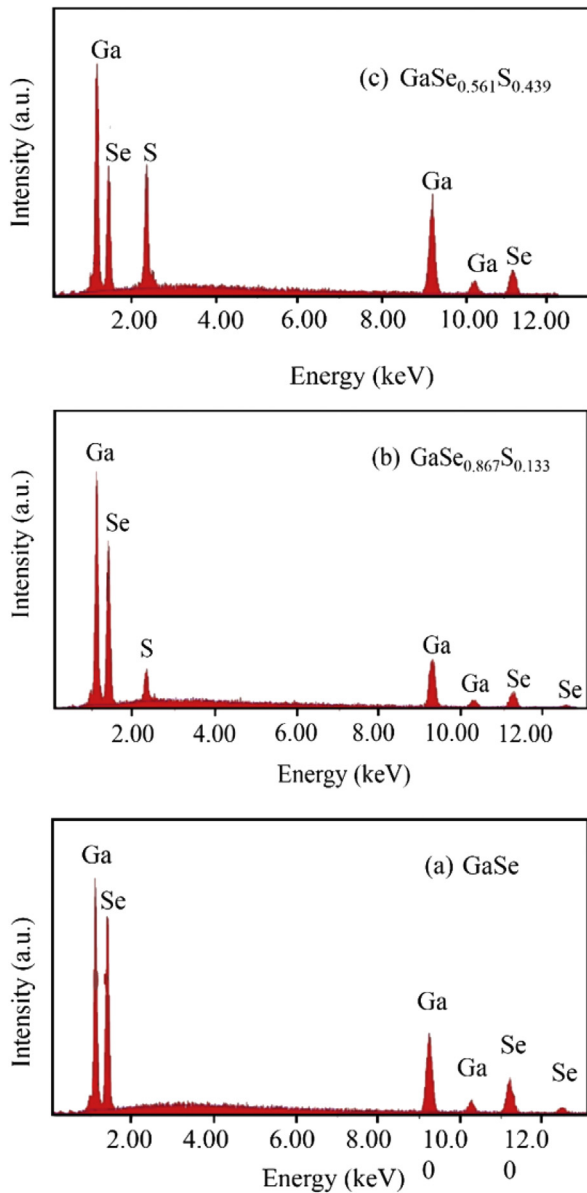

Fig. 5. EDS spectra revealing the increment of sulfur content in the GaSe$_{1-x}$S$_x$ crystals grown from the melt containing (a) 0 at %, (b) 3 at % and (c) 11 at % of sulfur ($x = 0$, 0.133 and 0.439, respectively).

3.2. Optical properties

The ellipsometric measurement technique is based on the analysis of the variation of the polarization parameters Ψ and Δ of the linearly polarized light beam after reflection from the sample surface. The ellipsometric data Ψ and Δ, which are related to the optical and structure properties of the sample, represent the amplitude ratio and phase shift of the parallel (p) and perpendicular (s) components of the reflected light. The complex reflectance ratio of the polarized light can be given as: $\rho = \frac{R_p}{R_s} = \tan\psi^{i\Delta}$, in which R_p and R_s are the complex reflection coefficient of the parallel and perpendicular directions of the polarized incident light, respectively [25]. Fig. 6 (a) and (b) show the Ψ and Δ spectra measured for GaSe$_{1-x}$S$_x$ ($x = 0$, 0.133, and 0.439) single crystals. One can find that the spectral features are strongly depend on the S-doping concentration. Due to the relatively thick (about 3 mm) GaSe$_{1-x}$S$_x$ single crystals, the semi-infinite medium approach can be used to directly derive the dielectric function from the experimental SE data according to the equation [26]:

$$\varepsilon_1 = (n_0 \sin\theta)^2 \times \left[1 + \tan^2\theta\,\frac{\cos^2 2\psi - \sin^2 2\psi\,\sin^2 2\Delta}{(1 + \sin 2\psi\,\cos\Delta)^2}\right], \qquad (2)$$

$$\varepsilon_2 = -(n_0 \sin\theta \tan\theta)^2 \times \frac{\sin 4\psi\,\sin\Delta}{(1 + \sin 2\psi\,\cos\Delta)^2}. \qquad (3)$$

where θ is the incident angle, and $n_0 = 1$.

The refractive index (n) and extinction coefficient (k) is related to the real and imaginary parts of the dielectric constant, which can be expressed by the relations: $\varepsilon_1 = n^2 - k^2$; $\varepsilon_2 = 2nk$. Fig. 6 (c) and (d) show the n and k spectra of the GaSe$_{1-x}$S$_x$ single crystals. The optical constants (n and k) spectra are similar to that observed in Ga$_{0.75}$In$_{0.25}$Se [27], GaSe$_{1-x}$Te$_x$ [28], and GaCr$_{0.1}$Se$_{0.9}$ [29] single crystals. However, the n values of GaSe$_{1-x}$S$_x$ single crystals are larger than that observed from Ga$_{0.75}$In$_{0.25}$Se while less than that obtained from GaSe$_{1-x}$Te$_x$ and GaCr$_{0.1}$Se$_{0.9}$ single crystals. It indicates that the doping elements and concentrations can affect the optical constants. Owing to the stoichiometry deviation, residual absorptions might exist at photon energies below the band gap energy. Therefore, the n values at the photon energy below 2 eV are not equal to zero. Moreover, from the extinction coefficient spectra, two critical peaks can be found at energies about 3.83 eV and 4.96 eV, which can be attributed to strong absorption of photon energy at the corresponding critical points. In addition, the peak positions blueshift with increasing the S concentration, which is associated with the change of electronic band structures.
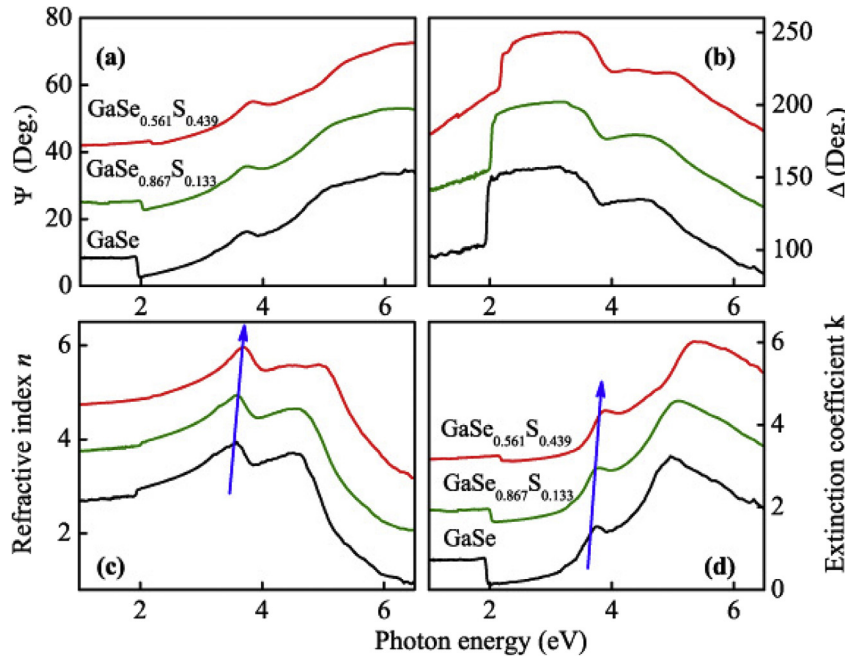
Fig. 6. The ellipsometric spectra (a) Ψ and (b) $\varDelta$ of the GaSe$_{1-x}$S$_x$ ($x=0$, 0.133, and 0.439) single crystals. The S concentration dependence of refractive index (c) n and extinction coefficient (d) k in the photon energy ranges from 1.03 to 6.52 eV. The arrows show the blueshift trends of critical peak positions.

3.3. Electronic transition

To obtain the accurate energies of critical point structures, the second derivatives of the complex dielectric functions can be fitted by the standard critical point (SCP) model. The expression of the model is given by:

$$\frac{d^2\varepsilon}{dE^2} = \begin{cases} n(n-1)A_m e^{i\Phi_m}(E - E_m + i\Gamma)^{n-2}, & n \neq 0, \\ A_m e^{i\Phi_m}(E - E_m + i\Gamma)^{-2}, & n = 0, \end{cases} \quad (4)$$

where A_m is the amplitude, Φ_m is the excitonic phase angle, E_m is the threshold energy, and Γ_m is the broadening parameter. The parameter m is the number of oscillators used in the fitting process. The exponent values $n = -1$, $-1/2$, 0 and 1/2 represent excitonic one, two, and three-dimensional line shapes, respectively. Since $n = -1$ case demonstrates the lowest mean-square deviations, the parameter n was set to -1 in this work and the spectra were fitted for the case of excitonic optical transitions. Because the second derivative values are very sensitive to small changes of the main data, the smoothing process should apply without distorting of the data recorded. However, since the smoothing process strongly distorts the main experimental data in the range of 2.0–3.0 eV, we accomplished the fitting process only for the region above 3.0 eV.

As an example, Fig. 7 (a) and (b) show the second derivative spectra of real ($d^2\varepsilon_1/dE^2$) and imaginary ($d^2\varepsilon_2/dE^2$) parts of the dielectric constant in GaSe$_{0.561}$S$_{0.439}$ single crystal. In the energy range from 3 to 6 eV, five critical points at about 3.181, 3.786, 4.628, 5.086, and 5.974 eV can be observed from the fitting results. The critical points conform to the results from Ga$_{0.75}$In$_{0.25}$Se [27] and GaSe [30] single crystals. The characteristics correspond to the different interband electronic transitions between filled and empty bands in the GaSe$_{0.561}$S$_{0.439}$ single crystal. To understand the physical origins of the electronic transitions, the electric band structures of the GaSe$_{1-x}$S$_x$ should be described. GaSe crystals belong to the point group symmetry and cleave readily along the {0001} plane, while GaS has a centrosymmetric structure 6/mm. For GaSe$_{1-x}$S$_x$ single crystals, the valence band can be divided into
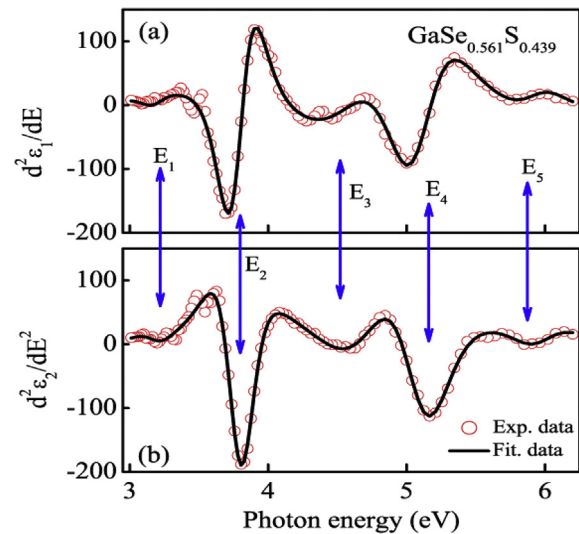
Fig. 7. Experimental (dots) and the best-fit (solid lines) second derivatives of ε_1 and ε_2 for the GaSe$_{0.561}$S$_{0.439}$ sample. The energies of each critical point are indicated by the arrows and labeled as E_1, E_2, E_3, E_4, and E_5, respectively.

three sub-bands. Low-lying conduction bands are located between 0.6 and 3.0 eV, which consist of mixtures of Se(S)-p, Ga-s and Ga-pz orbitals [31].

The E_1 transition can be assigned to the second highest valence band to the bottom of the conduction band. Furthermore, the E_2 critical point can be interpreted as the transition from the valence band maximum to the third group of the conduction band at the Brillouin zone center [30]. For the third transition at higher energy, it can be attributed to the electron excitations from the second highest valence band to the third group of conduction bands [32]. The E_3 structure can be also regarded as an interband transition related to larger Ga–Ga bond interactions. Many efforts have been made to interpret the origin of the critical points from 4.8 to 6 eV,

yet the origins are remaining uncertain. We believe that the E_4 and E_5 transitions are related to the excitation of electrons from the lower valence bands to the higher group of conduction bands.

Table 1 lists the critical point analysis results of the GaSe$_{1-x}$S$_x$ ($x = 0$, 0.133 and 0.439) single crystals. As can be seen in Table 1, the electronic transition energies shift to higher energies with increasing the S-doping concentration. This is because the electronic properties are sensitive to the inter-atomic distance of the semiconductor. With doping of S, the Se atoms will be replaced by S atoms. Considering that the S atoms are smaller than Se atoms and the ability for S atoms to attract electrons are stronger than that for Se atoms, the distance between S and Ga will be shorten leading to the decrease of D_{Ga-X} ($X = S$, Se) and the increase of D_{Ga-Ga} in GaSe$_{1-x}$S$_x$ single crystals [18]. The fact that electronic transition energies are increasing with the doping of the smallest cation or anions is in agreement with the observations from other semiconductor single crystals [33].

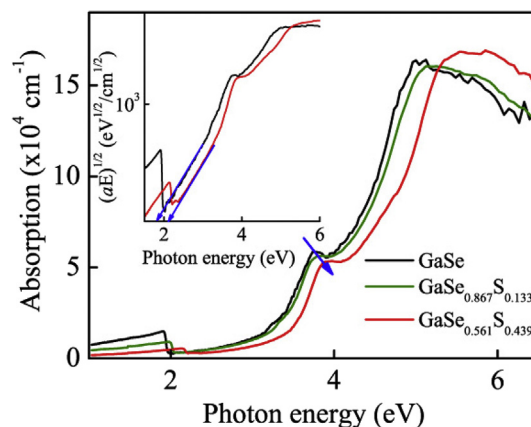### 3.4. Absorption characteristics

The absorption coefficient is one of the most important parameters for optoelectronic applications. To investigate the optical properties for further applications, the absorption coefficient ($\alpha = 4\pi k/\lambda$) of the GaSe$_{1-x}$S$_x$ single crystals ($x = 0$, 0.133 and 0.439) are depicted in Fig. 8, and it is found to be $0.17 \times 10^4 - 15 \times 10^4$ cm^{-1} in the wide spectral range from 1.03 to 6.52 eV. These values are larger than that reported for Al doped GaSe [34] and Te doped GaSe solid solutions [9]. With increasing the S or Al concentration, the absorption edges move toward the higher energy, while the absorption edge of Te doped GaSe single crystals moves toward the lower energy. Therefore, one can conclude that the band gap of GaS is larger than that of GaSe and GaTe. In addition, it can be observed that the absorption coefficient decreases with increasing the doping level. This is because the absorption coefficient of GaS is less than that of GaSe. In the transparency region, recorded absorption coefficient α for GaSe$_{1-x}$S$_x$ single crystals is ≤ 0.05 cm^{-1}. It is about three times lower than that for GaSe [9].

The power law behavior of $Tauc(\alpha E)^{\frac{1}{2}} \propto (E - E_g)$ is for allowed indirect transition [35], here E is the incident photon energy, and E_g is the OBG energy. So, the straight line between $(\alpha E)^{\frac{1}{2}}$ and E will provide the E_g value, which is extrapolated by the linear portion of the plot to $(\alpha E)^{\frac{1}{2}} = 0$. As examples, the inset of Fig. 8 shows the band gap values of the GaSe and GaSe$_{0.561}$S$_{0.439}$ single crystals (1.908 and 2.081 eV, respectively). This result indicates that the band gap features an energy blue-shift with increasing S concentration. The similar blue-shift phenomenon has been also reported by Wu et al. They found that the band gap moved from 1.986 eV (GaSe) to 2.370 eV (GaSe$_{0.5}$S$_{0.5}$) [36], which is larger than these results. The change of valence-band maxima and the conduction-band minima might be small for the lower S concentration. This evidence also indicates that the crystal phase and band-edge property for GaSe$_{1-x}$S$_x$ ($0 \leq \times \leq 0.5$) series solids are similar [32]. More systematic experiments are needed to verify this property. The increase of band gap energy indicates that the S-doping can change the electronic band structure of GaSe$_{1-x}$S$_x$ single crystals.

Fig. 8. The absorption coefficient α of the GaSe$_{1-x}$S$_x$ single crystals with different S concentrations. Inset shows variations of $(\alpha E)^{\frac{1}{2}}$ with the photon energy E, which are used to determine the optical band gap (E_g) of the GaSe and GaSe$_{0.561}$S$_{0.439}$ single crystals, respectively.

3.5. Electronic band structure and optical band gap

In order to further investigate the influences of S-doping on the band gaps of GaSe$_{1-x}$S$_x$, we calculate the electronic band structures of GaSe$_{1-x}$S$_x$ ($x = 0$, 0.133, and 0.439) with the first-principle calculations. Fig. 9(a) shows the band structure of pure GaSe crystal. One can find that the valence band maximum (VBM) is located at the Γ point, while the conduction band minimum (CBM) is located at M point. The calculation result reveals that the band gap of GaSe is about 2.065 eV, which agrees with Y. Fan's result [37]. For the GaSe$_{1-x}$S$_x$ ($x = 0.133$, and 0.439) crystals, the symmetry varies with the doping of S. To compare the change of the band structure, we use P_1 symmetry to calculate the S doping situation. The calculated band structures of GaSe$_{0.867}$S$_{0.133}$ and GaSe$_{0.561}$S$_{0.439}$ single crystals are shown in Figs. 9(b) and 5(c), respectively. It can be seen that all the VBMs locate at Γ point and CMBs locate at F point. The calculated band gap energy is 2.085 and 2.15 eV, respectively.

Fig. 9(d) shows the evolution of band gap with the S concentration, where both of the experimental and theoretical band gaps increase with the S concentration. As a well-known point of calculations based on density-functional theory, the calculated optical band gaps are underestimated by about 20%−30%, as compared to the experimental values. The increment of band gap can be explained from the perspective of band structure evolutions. Also, the fundamental E_g of GaSe is about 2 eV, while the fundamental E_g of GaS is about 3 eV. With the doping of S, the Se atoms will be replaced by smaller S atoms. Therefore, it is easy to know that the E_g of GaSe$_{1-x}$S$_x$ will locate between 2 eV and 3 eV, and the band gap will increase while increasing the concentration of S. Moreover, the increased band gap can be attributed to the increased states density of the conduction band and valence band with the doping of S.

4. Conclusions

In summary, optical properties and interband electronic transitions of GaSe$_{1-x}$S$_x$ ($x = 0$, 0.133, and 0.439) single crystals as a function of S concentration have been investigated by comparison of using spectroscopic ellipsometry and first-principle calculations. The dielectric functions and absorption coefficient in the photon energy of 1.03−6.52 eV have been obtained. Five electronic transitions energy E_1, E_2, E_3, E_4, and E_5 were assigned, respectively, at about 3.310 eV, 3.674 eV, 3.931 eV, 4.962 eV, and 5.500 eV for solid solution crystal GaSe$_{1-x}$S$_x$ ($x = 0.133$). It can be found that the

Table 1
Critical point energies for the GaSe$_{1-x}$S$_x$ ($x = 0$, 0.133, and 0.439) single crystals, which are extracted by fitting the second derivatives of dielectric functions with SCP model.

Sample	E_1 (eV)	E_2 (eV)	E_3 (eV)	E_4 (eV)	E_5 (eV)
$x = 0$	3.197	3.457	3.736	4.810	5.932
$x = 0.133$	3.310	3.674	3.931	4.962	5.500
$x = 0.439$	3.181	3.786	4.628	5.086	5.974

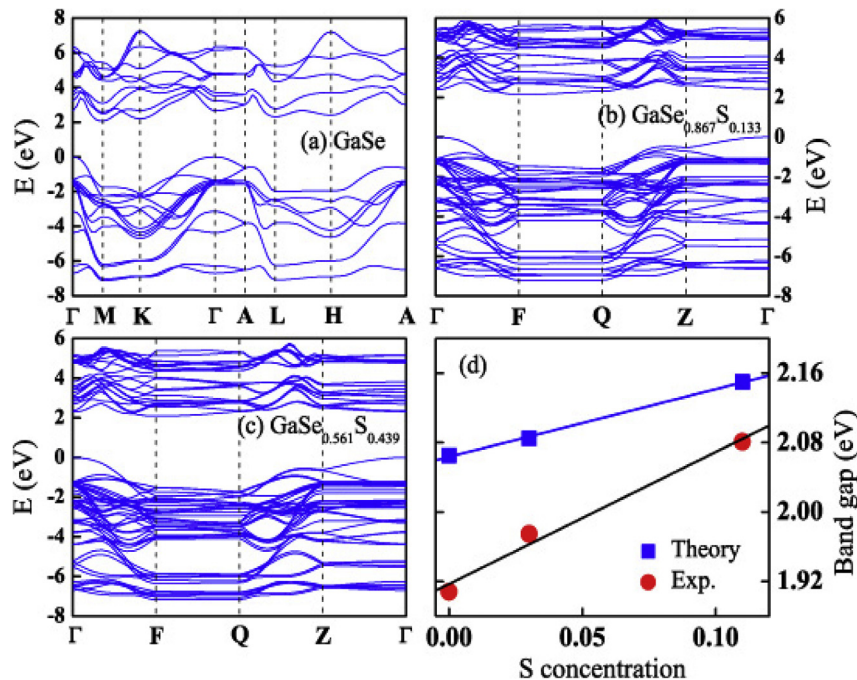**Fig. 9.** Calculated band structure of $GaSe_{1-x}S_x$ single crystals: (a) $x = 0$, (b) 0.133 and (c) 0.439; (d) the theoretical and experimental values of the band gap energy with increasing S concentrations.

transition energies of E_2, E_3, and E_4 increase with increasing the S concentration. Furthermore, the first-principle calculation results reveal that the band gap energy increases from 2.085 eV at $x = 0$ to 2.15 eV at $x = 0.439$, which is in good agreement with the SE experiment results (from 1.908 eV at $x = 0$ to 2.081 eV at $x = 0.439$).

References

[1] Y. Liu, N.O. Weiss, X.D. Duan, H.-C. Cheng, Y. Huang, X.F. Duan, Van der Waals heterostructures and devices, Nat. Rev. Mater. 1 (2016) 16042.
[2] K.S. Novoselov, A. Mishchenko, A. Carvalho, A.H. Castro Neto, 2D materials and Van der Waals heterostructures, Science 353 (2016) aac9439.
[3] W.G. Xu, W.W. Liu, J.F. Schmidt, W.J. Zhao, X. Lu, T. Raab, C. Diederichs, W.B. Gao, D.V. Seletskiy, Q.H. Xiong, Correlated fluorescence blinking in two-dimensional semiconductor heterostructures, Nature 541 (2017) 62–68.
[4] Z.P. Sun, A. Martinez, F. Wang, Optical modulators with 2D layered materials, Nat. Phot. 10 (2016) 227–238.
[5] M. Chhowalla, D. Jena, H. Zhang, Two-dimensional semiconductors for transistors, Nat. Rev. Mater. 1 (2016) 16052.
[6] W.W. Li, S.L. Li, K. Komatsu, A. Aparecido-Ferreira, Y.F. Lin, Y. Xu, M. Osada, T. Sasaki, K. Tsukagoshi, Realization of graphene field-effect transistor with high-k HCa$_2$Nb$_3$O$_{10}$ nanoflake as top-gate dielectric, Appl. Phys. Lett. 103 (2013) 023113.
[7] P. Tonndorf, S. Schwarz, J. Kern, I. Niehues, O.D. Pozo-Zamudio, A.I. Dmitriev, A.P. Bakhtinov, D.N. Borisenko, N.N. Kolesnikov, A.I. Tartakovskii, S.M.D. Vasconcellos, R. Bratschitsch, Single-photon emitters in GaSe, 2D Mater. 4 (2017) 021010.
[8] L. Hu, X.R. Huang, D.S. Wei, Layer-independent and layer-dependent nonlinear optical properties of two-dimensional GaX (X = S, Se, Te)
[9] nanosheets, Phys. Chem. Chem. Phys. 19 (2017) 11131.
[9] J. Guo, J.J. Xie, D.J. Li, G.L. Yang, F. Chen, C.R. Wang, L.M. Zhang, Y.M. Andreev, K.A. Kokh, G.V. Lanskii, V.A. Svetlichnyi, Doped GaSe crystals for laser frequency conversion, Light Sci. Appl. 4 (2015), e362.
[10] M. Isik, N. Gasanly, Ellipsometric study of optical properties of GaS$_x$Se$_{1-x}$ layered mixed crystals, Opt. Mater. 54 (2016) 155–159.
[11] Y.H. Wang, Y.M. Wang, J.D. Lu, L.L. Ji, R.G. Zang, R.W. Wang, Nonlinear optical properties of Cu nanoclusters by ion implantation in silicate glass, Opt. Commun. 283 (2010) 486–489.
[12] X.X. Yu, Y.H. Wang, Measurement of nonlinear optical refraction of composite material based on sapphire with silver by Kerr-lens autocorrelation method, Opt. Express 22 (2014) 177–182.
[13] H. Cheng, Y.H. Wang, H.W. Dai, J.B. Han, X.C. Li, Nonlinear optical properties of PbS colloidal quantum dots fabricated via solvothermal method, J. Phys. Chem. C 119 (2015) 3288–3292.
[14] C. Lin, X. Wu, M. Lin, Y.P. Huang, J. Li, Optical, luminescent and optical temperature sensing properties of (K$_{0.5}$Na$_{0.5}$)NbO$_3$-ErBiO$_3$ transparent ceramics, J. Alloy. Compd. 706 (2017) 156–163.
[15] H.P. Zhao, J.L. Tang, Q.S. Lai, G. Cheng, Y.L. Liu, R. Chen, Enhanced visible light photocatalytic performance of Sb-doped (BiO)$_2$CO$_3$ nanoplates, Catal. Commun. 58 (2015) 190–194.
[16] Z. Dai, F. Qin, H.P. Zhao, J. Ding, Y.L. Liu, R. Chen, Crystal defect engineering of aurivillius Bi$_2$MoO$_6$ by Ce doping for increased reactive species production in photocatalysis, ACS Catal. 6 (2016) 3180–3192.
[17] P.P. Dey, A. Khare, Stoichiometry-dependent linear and nonlinear optical properties of PLD SiO$_x$ thin films, J. Alloy. Compd. 706 (2017) 370–376.
[18] C.B. Huang, H.X. Wu, Y.B. Ni, Z.Y. Wang, M. Qi, C.L. Zhang, First-principles calculation of the structural, electronic, elastic, and optical properties of sulfur-doping ε-GaSe crystal, Chin. Phys. B 25 (2016) 086201.
[19] K.A. Kokh, J.F. Molloy, M. Naftaly, Yu.M. Andreev, V.A. Svetlichnyi, G.V. Lanskii, I.N. Lapin, T.I. Izaak, A.E. Kokh, Growth and optical properties of solid solution crystals GaSe$_{1-x}$S$_x$ crystals, Mater. Chem. Phys. 154 (2015) 152–157.
[20] G. Kressea, J. Furthmuller, Efficiency of ab-initio total energy calculations for metals and semiconductors using a plane-wave basis set, Comput. Mater. Sci. 6 (1996) 15–50.
[21] D.M. Ceperley, B.J. Alder, Ground state of the electron gas by a Stochastic method, Phys. Rev. B 45 (1980) 566–569.
[22] G. Kresse, D. Joubert, From ultrasoft pseudopotentials to the projector augmented-wave method, Phys. Rev. B 59 (1999) 1758–1775.
[23] F. Tran, P. Blaha, Accurate band gaps of semiconductors and insulators with a semilocal exchange correlation potential, Phys. Rev. B 102 (2009) 226401.
[24] A.D. Becke, E.R. Johnson, A simple effective potential for exchange, J. Chem. Phys. 124 (2006) 221101.
[25] J.M. Park, D.W. Lynch, S.J. Lee, D.L. Schlagel, T.A. Lograsso, A.O. Tsokol, J.E. Snyder, D.C. Jiles, Spectroscopic ellipsometry study of optical anisotropy in Gd$_5$Si$_2$Ge$_2$ and comparison with reflectance difference spectra, Phys. Rev. B 73 (2006) 035110.

[26] J.M. Chalmers, P.R. Griffiths, Handbook of Vibrational Spectroscopy, Chapter: Infrared Spectroscopic Ellipsometry, John Wiley & Sons Ltd, Chichester, 2002, p. 9.

[27] M. Isik, S.S. Cetin, N.M. Gasanly, S. Ozcelik, Optical constants of layered structured $Ga_{0.75}In_{0.25}Se$ crystals from the ellipsometric measurements, Solid State Commun. 152 (2012) 791—793.

[28] S.Yu. Sarkisov, V.V. Atuchin, T.A. Gavrilova, V.N. Kruchinin, S.A. Barezneya, Z.V. Korotchenko, O.P. Tolbanov, A.I. Chernyshev, Growth and optical parameters of GaSe:Te crystals, Russ. Phys. J. 53 (2010) 346—352.

[29] V.V. Atuchin, S.A. Bereznaya, N.F. Beisel, Z.V. Korotchenko, V.N. Kruchinin, L.D. Pokrovsky, A.I. Saprykin, S.Y. Sarkisov, Growth, chromium distribution and electrical properties of GaSe:Cr single crystals, Mater. Chem. Phys. 146 (2014) 12—17.

[30] S.G. Choi, D.H. Levi, C. Martinez-Tomas, V. Munoz Sanjose, Above-bandgap ordinary optical properties of GaSe single crystal, J. Appl. Phys. 106 (2009) 053517.

[31] J. Hong, D. Vanderbilt, First-principles theory and calculation of flexoelectricity, Phys. Rev. B 88 (2013) 174107.

[32] S.G. Choi, D.E. Aspnes, A.L. Fuchser, C. Martinez-Tomas, V.M. Sanjose, D.H. Levi, Ellipsometric study of single-crystal γ-InSe from 1.5 eV to 9.2 eV, Appl. Phys. Lett. 96 (2010) 181902.

[33] S.G. Choi, Y.D. Kim, S.D. Yoo, D.E. Aspness, D.H. Woo, S.H. Kim, Optical properties of $Al_xGa_{1-x}P$ (0.6 ≤x≤0.52) alloys, J. Appl. Phys. 87 (2000) 1287.

[34] J. Guo, J.J. Xie, L.M. Zhang, K. Kokh, Yu. Andreev, T. Izaak, G. Lanskii, A. Shaiduko, V. Svetlichnyi, Characterization of optical quality of GaSe:Al crystals by exciton absorption peak parameters, J. Mater. Sci. Mater. Electron. 25 (2014) 1757—1760.

[35] W.W. Li, J.J. Zhu, X.F. Xu, K. Jiang, Z.G. Hu, M. Zhu, J.H. Chu, Ultraviolet-infrared dielectric functions and electronic band structures of monoclinic VO_2 nanocrystalline film: temperature-dependent spectral transmittance, J. Appl. Phys. 110 (2011) 013504.

[36] C.C. Wu, C.H. Ho, W.T. Shen, Z.H. Cheng, Y.S. Huang, K.K. Tiong, Optical properties of $GaSe_{1-x}S_x$ series layered semiconductors grown by vertical Bridgman method, Mater. Chem. Phys. 88 (2004) 313—317.

[37] Y. Fan, M. Bauer, L. Kador, Photoluminescence frequency up-conversion in GaSe single crystals as studied by confocal microscopy, J. Appl. Phys. 91 (2002) 1081.